Talanta 118 (2014) 231–237

Contents lists available at ScienceDirect

Talanta

journal homepage: www.elsevier.com/locate/talanta

Preparation and characterization of magnetic nanoparticles for the on-line determination of gold, palladium, and platinum in mine samples based on flow injection micro-column preconcentration coupled with graphite furnace atomic absorption spectrometry

Juanjuan Ye [a], Shuxia Liu [a], Miaomiao Tian [a], Wanjun Li [a], Bin Hu [b], Weihong Zhou [a], Qiong Jia [a,*]

[a] College of Chemistry, Jilin University, Changchun 130012, PR China
[b] State Key Laboratory of Inorganic Synthesis and Preparative Chemistry, College of Chemistry, Jilin University, Changchun 130012, China

ARTICLE INFO

Article history:
Received 13 July 2013
Received in revised form
9 October 2013
Accepted 13 October 2013
Available online 18 October 2013

Keywords:
Crown ether-functionalized magnetic nanoparticles
Flow injection
Preconcentration
Graphite furnace atomic absorption spectrophotometry
Precious metals

ABSTRACT

A simple and highly selective procedure for on-line determination of trace levels of Au, Pd, and Pt in mine samples has been developed using flow injection-column adsorption preconcentration coupled with graphite furnace atomic absorption spectrophotometry (FI-column-GFAAS). The precious metals were adsorbed on the as-synthesized magnetic nanoparticles functionalized with 4′-aminobenzo-15-crown-5-ether packed into a micro-column and then eluted with 2% thiourea+0.1 mol L^{-1} HCl solution prior to the determination by GFAAS. The properties of the magnetic adsorbents were investigated by scanning electron microscope (SEM), X-ray diffraction (XRD), and vibrating sample magnetometer (VSM). Various experimental parameters affecting the preconcentration of Au, Pd, and Pt were investigated and optimized. Under the optimal experimental conditions, the detection limits of the developed technique were 0.16 ng mL^{-1} for Au, 0.28 ng mL^{-1} for Pd, and 1.01 ng mL^{-1} for Pt, with enrichment factors of 24.3, 13.9, and 17.8, respectively. Precisions, evaluated as repeatability of results, were 1.1%, 3.9%, and 4.4% respectively for Au, Pd, and Pt. The developed method was validated by the analysis of Au, Pd, and Pt in certified reference materials and mine samples with satisfactory results.

1. Introduction

Direct determinations of trace or ultra-trace levels of metals in geological, metallurgical, and environmental samples are difficult because of their extremely low concentrations together with very complicated sample matrices [1,2]. Thus, a separation and preconcentration procedure is required even with the high sensitivity and selectivity of modern analytical techniques, such as graphite furnace atomic absorption spectrometry (GFAAS) [3,4], inductively coupled plasma optical emission spectrometry (ICP-OES) [5–7], inductively coupled plasma mass spectrometry (ICP-MS) [8–10], adsorptive stripping voltammetry (ASV) [11] or neutron activation analysis (INAA) [12]. Although GFAAS shows similar shortcomings, it is available in most laboratories and has a chance to be in common use over traditional atomic spectrometries. In order to achieve sensitive and reliable results, separation and preconcentration of analytes from the matrix is often necessary prior to GFAAS determinations.

Precious metals have a wide range of potential applications including biological activity, catalysis, jewelry, chemical industry, and surface technology because of their specific physical and chemical properties [13–16]. Due to their low abundance in the earth and their high economic values, several classical separation and preconcentration methods, such as coprecipitation [17], liquid–liquid extraction [4,18], membrane filtration [19], ion-exchange [8], and adsorption [13,20–26] were adopted. Although liquid–liquid extraction can be used to selectively remove precious metals from solutions, it is a time-consuming procedure and requires large quantities of organic solvents. Adsorption seems to be a more suitable method for the separation and preconcentration of precious metals due to simply operating, no or little use of organic solvents, and high efficiency. There are various adsorbents including activated carbon [20,21], biosorbent [15,22], and ion exchange resin [24]. Recently, more and more attention has been gained in the field of sample extraction by magnetic nanomaterials [27–29] due to their unique magnetic response, large surface area, and chemically modifiable surface [30,31]. When organic extractants are modified on the magnetic nanomaterials, the obtained extractant-coated magnetic adsorbents can be packed, dynamically positioned, and repacked in micro-columns by using an external magnetic field placed outside of the extraction container. The whole operation process does not need additional centrifugation or filtration of the sample, which makes sampling and collection easier and faster [32]. To reduce the

* Corresponding author. Tel.: +86 431 85095621.
E-mail address: jiaqiong@jlu.edu.cn (Q. Jia).

0039-9140/$ - see front matter © 2013 Elsevier B.V. All rights reserved.
http://dx.doi.org/10.1016/j.talanta.2013.10.018

separation time and eliminate the interferences, the extraction and back-extraction steps can be conducted simultaneously if a flow injection technique (FI-column) is used with a micro-column packed with the magnetic adsorbent [27].

Macrocyclic compounds, due to their selective receptor properties and ease of structural modification, have been employed as complexing agents to form stable and selective complexes with alkali, alkaline earth metals, and ammonium cations [33,34]. The high selectivity of macrocycles can be utilized in separation chemistry, such as ion chromatography [33], ion selective electrodes [35], and solvent extraction [36]. 4′-Aminobenzo-15-crown-5-ether (AB15C5), as a benzo condensed crown compound, has the similar chemical properties as solvent extraction reagent, which can prompt crown ether to effectively adsorb analytes through electrostatic and conformational effects, and subsequently coordinate the pairing ion [37]. The combination of magnetic particle and crown ether has potential as a new strategy for the extraction of metal ions and ion pair species, which can incorporate the advantages of magnetic materials and benzo condensed crown compounds. However, to our knowledge, there are no reports about applications of magnetic AB15C5 nanoparticles as sorbents.

In the present work, the crown ether-coated magnetic nanoparticles (hereafter abbreviated as CEMNs) were prepared and used as the adsorption materials for FI-column separation and preconcentration before GFAAS determinations of Au, Pd, and Pt. The synthesized CEMNs possessed high extraction efficiency owing to the nanosize and the abundant functional groups. In order to achieve the best analytical performance, several experimental parameters, such as NaCl concentration, sample pH value, sample loading time, sample flow rate, eluent concentration, and eluent flow rate were optimized. Meanwhile, the accuracy and selectivity of the proposed method were demonstrated by the determination of Au, Pd, and Pt in certified reference mine materials and real geological samples under the optimized conditions.

2. Experimental

2.1. Reagents and materials

The intermediate Au, Pd, and Pt working standard solutions (10 mg L^{-1}) were prepared by appropriate dilution of the stock solutions, 1000 mg L^{-1} for Au (III), Pd (II), and Pt (IV), from Beijing NCS Analytical Instruments Co. Ltd. (Beijing, China, http://www.ncscrm.com). The stock solutions were stored at 4 °C. A series of working standard solutions of the above mentioned elements were daily prepared by dilution of the appropriate amount of stock solutions in 0.1 mol L^{-1} HCl. (3-Aminopropyl) triethoxysilane (APTES, 99%) and sodium cyanoborohydride ($NaBH_3CN$) were purchased from Aladdin Reagent Co. Ltd., China. Certified reference materials, GAu-11b, GBW07289, GBW07291, and GBW07292, were obtained from the National Research Center for Standard Materials (Beijing, China). The geological samples were collected from Heilongjiang province (Heilongjiang, China). All used reagents were of the highest available purity or at least analytical reagent grade. Deionized purified water (DDW) was prepared by the Milli-Q SP system (Millipore, Milford, MA, USA).

2.2. Apparatus

The experiments were performed using a Shimadzu AA-6300C atomic absorption spectrophotometer equipped with a graphite furnace atomizer GFA-EX7i and an auto-sampler ASC-6100 (Shimadzu, Japan). The hollow cathode lamps and pyrolytic-coated graphite tubes (Shimadzu part no. 206-50588) were used. Deuterium background correction was employed to correct non-specific absorbances. The sample injection volume was 20 μL in all experiments, and output signals were collected and processed in continuous peak height mode. The operating instrumental parameters for all studied elements are listed in Table 1. A model IFIS-D flow injection system (Remex Analyse Instrument Co. Ltd., Xi'an, China) was employed for the separation and preconcentration of precious metals, with the FI manifold shown in Fig. 1. The IFIS-D consisted of two peristaltic pumps, a standard rotary injection valve (8-channel, 16-way rotary injection valve, multifunctional injector), and PTFE tubes (0.8 mm i.d.), with which the sample and reagents were delivered to minimize the dead volume as short as possible. A glassy micro-column (50 mm × 3 mm i.d., Beion Medical Technology Co. Ltd., Shanghai, China) was used for packing the CEMNs. A PB-10 digital pH meter (Sartorius Scientific Instruments Co. Ltd., Beijing, China) was employed for pH measurements.

JSM 6700-F (JEOL Company, Japan) was used to characterize surface morphology of nanocomposites. The structure analysis of the magnetic nanoparticle was carried out using an X-ray Diffractometer (R-AXIS RAPID-F, Rigaku Corporation, Japan) with a detector operating under a voltage of 40.0 kV and a current of 30.0 mA using Cu Kα radiation, and the recorded range of 2θ was 20–80°. The magnetic

Table 1
GFAAS operating parameters.

	Wavelength (nm)	Slit width (nm)	Current (mA)	Temperature (°C)				Time (s)			
				Dry	Pyrolysis	Atomizaition	Cleaning	Dry	Pyrolysis	Atomizaition	Cleaning
Au	242.8	0.7	10	150–250	700–700–700	2100	2500	10–10	10–10–3	4	2
Pd	247.6	0.7	10	150–250	1000–1000–1000	2700	2800	20–30	10–10–3	2	2
Pt	265.9	0.7	14	120–250	1200–1200–1200	2600	2650	20–10	10–10–3	3	2

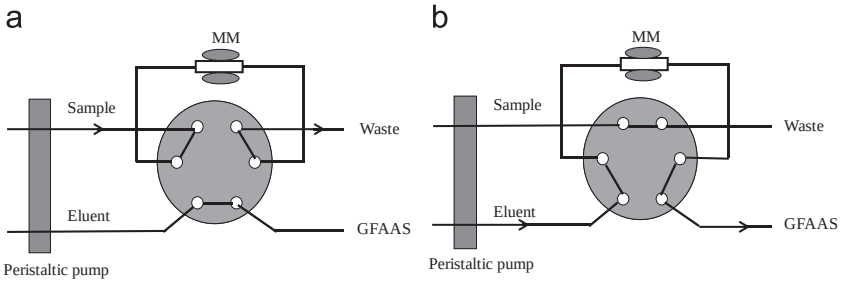

Fig. 1. Diagram of the flow injection procedure. MM, magnetic micro-column and magnet. (a) Load position, (b) Injection position.

property was estimated using a Superconducting Quantum Interference Device (MPMS SQUID XL-7, Quantum Design, USA).

2.3. Procedures

2.3.1. Preparation of Fe_3O_4@SiO_2 microspheres

The magnetic Fe_3O_4 nanoparticles were synthesized through a solvothermal reaction according to previous methods [32]. Then, as-synthesized Fe_3O_4 powder (0.2 g) was treated with 0.1 mol L^{-1} HCl. After getting separated from the aqueous solution and cleaned with DDW, the magnetite particles were re-dispersed in a mixture of ethanol (100 mL), DDW (20 mL), and concentrated ammonia aqueous solution (1.0 mL). Subsequently, 0.2 mL tetraethoxysilane was quickly added to the above prepared dispersion with vigorous stirring and the reaction was allowed to proceed for 6 h at room temperature. Finally, the obtained Fe_3O_4@SiO_2 microspheres were separated and rinsed with ethanol by use of a magnet, and then dried in a vacuum at 60 °C for 6 h.

2.3.2. Preparation and modification of Fe_3O_4@SiO_2 microspheres for crown ether immobilization

APTES was first used to functionalize Fe_3O_4@SiO_2 microspheres with an alkylamine group [38]. 0.6 g Fe_3O_4@SiO_2 microspheres were mixed by vigorous stirring with 45 mL dried toluene in a 250 mL three-neck flask equipped with a reflux condensing tube. After the particles were well dispersed, 4 mL APTES was added slowly to the flask under continuous mechanical stirring. The reaction continued under reflux for 4 h at 95 °C. The resulting particles were cooled to room temperature, and collected with a magnet. After being washed with dried toluene, water, and ethanol, the Fe_3O_4@SiO_2@APTES particles were dried in a vacuum oven at room temperature.

Glutaraldehyde (GA) was used as the activating agent for the coupling of the AB15C5 to amine groups of the magnetic microspheres [39]. The above Fe_3O_4@SiO_2@APTES particles were added to 39.0 mL 0.1 mol L^{-1} phosphate buffer (pH=8.0) and 0.8 mL GA (25%, v/v), and the solution was carried out at 25 °C with orbital shaking (90 rpm) for 15 min. The aldehyde-activated magnetic microspheres were rinsed with phosphate buffer solution by using a magnet. Then, 0.12 g AB15C5 in 20 mL 0.1 mol L^{-1} phosphate buffer pH 8.0 was added. $NaBH_3CN$ reduction was performed to convert unstable Schiff's bases into stable secondary amines. After 1 h, 0.06 g $NaBH_3CN$ was added to the above solution. The coupling reaction was then performed for 7 h at 25 °C with orbital shaking (90 rpm). Finally, phosphate buffer solution and ethanol were used to wash the CEMNs and were then dried in a vacuum oven at 60 °C for 6 h.

2.3.3. Preparation of micro-column

Before use, 20 mL 10% (v/v) HCl and 20 mL DDW were passed through the micro-column successively at a flow rate of 3.0 mL min^{-1} to clean any inorganic compounds. 50 mg magnetic CEMNs were packed into the micro-column, leading to a packing bed due to the strong magnetic field. The sorbent was flushed with DDW, 2% (v/v) thiourea (TU)+0.1 mol L^{-1} HCl, and DDW to remove the remaining TU+HCl solution.

2.3.4. Adsorption and elution experiments

The FI manifolds used are shown in Fig. 1, and the details on the operation sequence of the FI on-line separation and preconcentration experiment are as follows. The above prepared micro-column of CEMNs was fixed by an external magnetic field. In the preconcentration step, the injection valve was in the "Load" position, the blank solution was pumped into the micro-column with a flow rate of 3.0 mL min^{-1} for 30 s to eliminate the eluent that remained from the last elution. Then, the sample solutions containing 1 ng mL^{-1} Au, 2 ng mL^{-1} Pd, and 5 ng mL^{-1} Pt were loaded onto the micro-column with a flow rate of 3.0 mL min^{-1} for 2 min. The analytes were adsorbed and other ions were directed to wastes. Subsequently, the blank solution was driven through the micro-column for 30 s to remove the residual sample matrices. In the elution step, the valve was turned to the "Injection" position, and the eluent was pumped through the micro-column for eluting the analytes adsorbed on the micro-column with a flow rate of 1.0 mL min^{-1} for 30 s. Lastly, the eluent solution was introduced into the GFAAS. The variable FI parameters affecting the on-line separation process were carried out in triplicate and the average results were presented.

In order to make full use of the prepared micro-column of CEMNs, it was reused after regeneration with the eluent of 2% TU+0.1 mol L^{-1} HCl and DDW, respectively. The same micro-column could be used repeatedly under the optimized experimental conditions after 400 successive adsorption–elution operations. The stability of the adsorption properties of the micro-column had no significant changes.

2.3.5. Sample pretreatment

Portions (5.0 or 10.0 g) of the certified reference samples or mine samples were placed in a porcelain crucible, roasted in an electric muffle furnace at 650 °C for 2 h. Then the crucible was taken out and cooled down to room temperature. The sample was transferred into beakers and pretreated with 50 mL aqua regia for about 1 h while being heated on an electric hot-plate, and evaporated to moist salt state, successively. The final residues were washed with 1% HCl several times, and the washings were

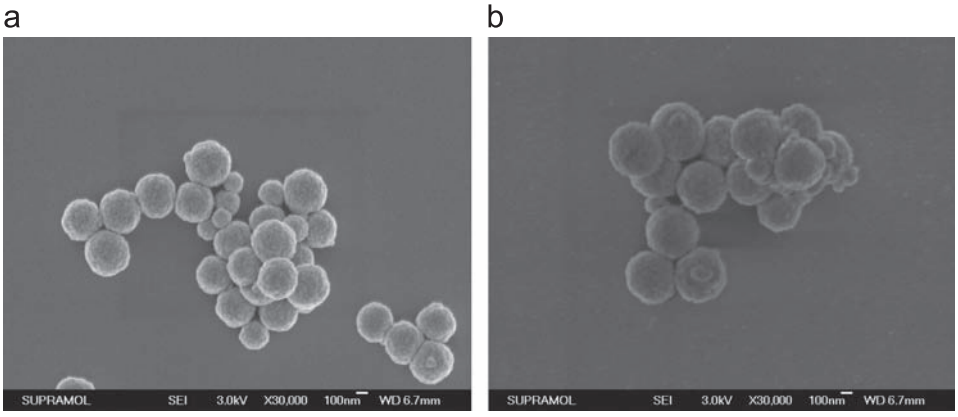

Fig. 2. SEM images of the Fe_3O_4 nanoparticles (a) and CEMNs (b).

transferred into a 50 mL volumetric flask. The filtrate was adjusted to volume with DDW.

3. Results and discussion

3.1. Identification of magnetic nanoparticle

3.1.1. SEM

The SEM images of the Fe_3O_4 and the CEMNs are illustrated in Fig. 2. The morphology of the microspheres revealed that CEMNs were spherical particle with an average diameter of around 350 nm, which was slightly larger than that of Fe_3O_4 microspheres after modification. Due to the polymerization reaction, the surface of CEMNs was relatively rough. However, the post-surface modification processes did not have effect on their monodispersity and morphology of the magnetic microspheres.

3.1.2. X-ray diffraction spectrum

The crystal phases and purity of the obtained magnetic nanoparticles were determined by XRD. As shown in Fig. 3, the 2θ diffraction peak of the unmodified magnetic nanoparticles appeared at 30.3°, 35.5°, 43.3°, 53.4°, 57.1°, and 62.8°, with the XRD peak position and intensity of the nanocrystallite matching well with standard Fe_3O_4 and without other crystal phases detected, according to the JCPDS card no. 19-629. By comparing the spectrum of Fig. 3a and b, the XRD analysis of CEMNs indicated six characteristic peaks at the same positions, revealing that the coating process did not result in the crystal structure variation of Fe_3O_4.

3.1.3. Magnetic properties using SQUID

Magnetization measurements are commonly performed to investigate the surface modified magnetic nanoadsorbents in the magnetic separation. Magnetic hysteresis loops shown in Fig. 4 confirmed the magnetic behaviors of Fe_3O_4 and CEMNs at room temperature. The maximum saturation magnetization value of CEMNs was determined as 53.3 emu g^{-1}. This value was lower than that of the corresponding bulk Fe_3O_4 (61.9 emu g^{-1}), which may be due to the fact that CEMNs declined with the surface modification slightly and led to a decrease in the saturation magnetization. The magnetic separability of such magnetic particles was tested in ethanol by placing a small neodymium permanent magnet near the glass bottle. The black particles were attracted toward the magnet for a few seconds, demonstrating that the CEMNs possessed good magnetic response, and could be efficiently separated from the solution under an external magnetic field.

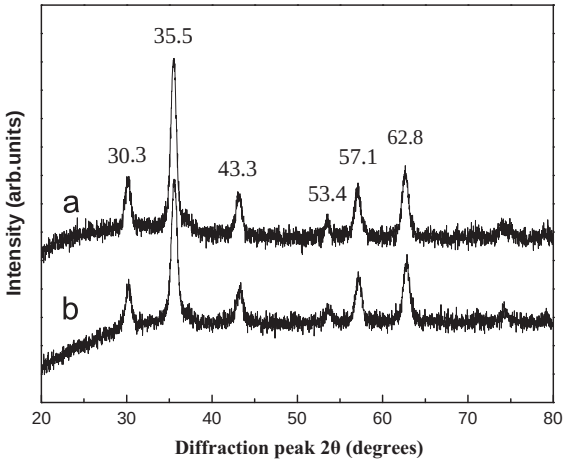

Fig. 3. X-ray diffraction pattern of the Fe_3O_4 nanoparticles (a) and CEMNs (b).

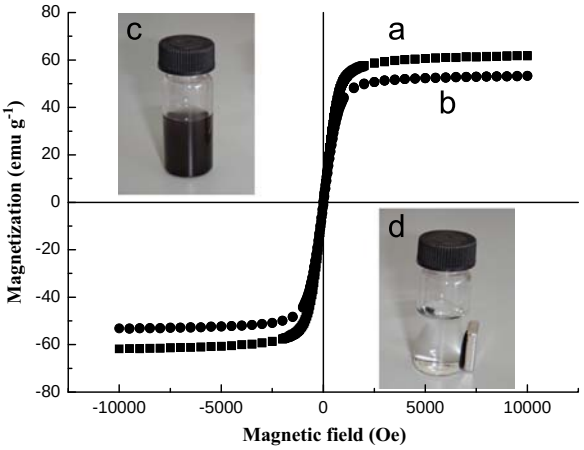

Fig. 4. Magnetic hysteresis loops of the Fe_3O_4 nanoparticles (a) and CEMNs (b) obtained recorded at room temperature. Photographs of the ethanol dispersion of CEMNs before (c) and after separation with a magnet for a few seconds (d), indicating a fast separation process of the microspheres in the dispersion.

3.2. Effect of experimental variables

3.2.1. Effect of NaCl concentration

The effect of sodium chloride concentration is one of the most important parameters that should be considered for the preconcentration process. Because AB15C5 modified on the magnetic particles can form a complex with metal ions, which is normally related to the ratio of the cavity to the cation radius, especially with sodium cation [40,41], and Au, Pd, and Pt can form strong complex anions with Cl^- in solution [42,43].

$$Na^+ + AB15C5 \Leftrightarrow Na^+\text{–}AB15C5$$

$$Na^+\text{–}AB15C5 + X^{n-} \Leftrightarrow Na^+\text{–}AB15C5\text{–}X^{n-}$$

($X^{n-} = AuCl_4^-$, $PdCl_4^{2-}$, and $PtCl_6^{2-}$)

These abilities were used for concentrating these precious metal complex anions (X^{n-}) with the positively charged sodium complex of AB15C5 (Na^+–AB15C5) by on-line formation of cooperative ion-pair binding effects. At the same time, the adsorption in the form of such complex also reduces the interference from other transition metals for precious metals. The effect of NaCl concentration on the integrated absorbance of precious metals was studied in the range 0–0.3% (m/v). As shown in Fig. 5, the analytical signal increased with the increasing concentration of NaCl and then leveled off. So 0.05% (m/v) NaCl was selected for further experiments.

3.2.2. Effect of sample pH

As another significant factor which has a great effect on the adsorption efficiency of the precious metal ions, sample pH was investigated at the NaCl concentration of 0.05% (m/v). The sorption of analytes was examined in the pH range of 1.0–7.0 which was adjusted by 1.0 mol L^{-1} HCl or 0.01 mol L^{-1} NaOH. The results are presented in Fig. 6a. When pH is too low, a portion of oxygen atoms of crown ether may be protonated due to the competitive adsorption between hydrogen ions and sodium ions, which is not advantageous for the precious metal adsorption. The optimal pH was found to be between 2.0 and 4.0, and the adsorption amount decreased with the increase in pH, which was attributed to the hydrolysis at relative high pH values. Because the types of the metal ion complexes greatly affect their adsorption behaviors in aqueous solutions, the predominant complex of precious metal complexes are $AuCl_4^-$, $PdCl_4^{2-}$, and $PtCl_6^{2-}$ at low pH values (below 3.0) in chloride medium [42,43]. This phenomenon may be

primarily attributed to the electrostatic attraction between the negatively charged X^{n-} and the positively charged Na^{+}–AB15C5 in the form of the Na^{+}–AB15C5–X^{n-} at lower pH values. Meanwhile, X^{n-} can be adsorbed on the micro-column with the protonated amino groups of the CEMNs through electrostatic attraction at low pH. Since the maximum adsorption capacity occurred at pH of 2.0, the following adsorption studies were carried out at pH 2.0 as the preconcentration medium for Au, Pd, and Pt.

3.2.3. Effect of sample loading time

In order to obtain higher enrichment factor, the influence of sample loading time on the absorbance was investigated. Results indicated that the integrated absorbance of analytes increased with long loading time in the range of 0.5–3.5 min at a constant sample flow rate. Although longer loading time is a crucial parameter to increase the adsorption capacity, it can reduce the analytical frequency which affects the efficiency of the method, and use larger volumes of sample. Taking this into consideration, an optimized loading time of 2.0 min was used in the present work.

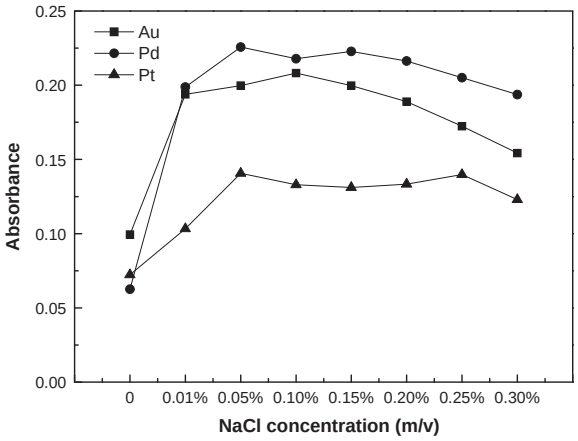

Fig. 5. Effect of NaCl concentration on the absorbance. Sample pH: 2.0; sample loading time: 2.0 min; sample flow rate: 3.0 mL min^{-1}; eluent: 2% TU+0.1 mol L^{-1} HCl; eluent flow rate: 1.0 mL min^{-1}.

3.2.4. Effect of sample flow rate

The effect of sample flow rate on the absorbance was studied in the range from 0.5 to 4.0 mL min^{-1} by keeping other experimental conditions fixed. The experimental results in Fig. 6b stated that satisfactory signals of absorbance were found when the flow rate was relatively high. However, flow rate in higher level needs stronger pressure, which may damage the pipelines and leaks in the system. Moreover, the signal of Pt increased slightly when the sample flow rate was greater than 3.0 mL min^{-1}, the analyte may not be preconcentrated efficiently on the micro-column and may be partly lost. Consequently, a sample flow rate of 3.0 mL min^{-1} was adopted.

3.2.5. Effect of eluent

In order to ensure an effective elution of the absorbed analytes on the micro-column, TU and HCl were employed as the eluent in the present work. The concentration of TU on the absorbance was investigated in the range of 0–5.0% (Fig. 6c). It showed that Au could be eluted efficiently with a TU concentration range of 0.5–3.0%, while Pd with a concentration range of 1.5–3.0%. The absorbance of Pt achieved its maximum value when 5.0% TU solution was used. The effect of acid at concentrations of 0.1–2.0 mol L^{-1} had a slight influence on the absorbance of Pt, which decreased with the increase of HCl concentration. The maximum

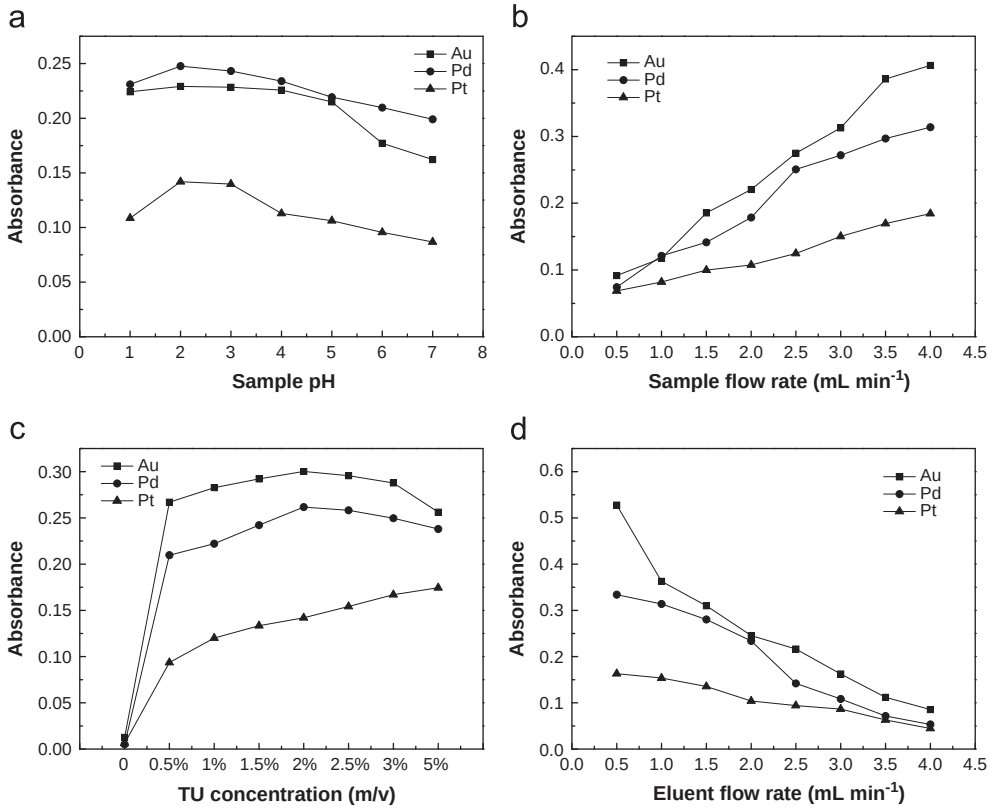

Fig. 6. Effect of experiment conditions on the absorbance. Standards: 1 ng mL^{-1} Au, 2 ng mL^{-1} Pd, and 5 ng mL^{-1} Pt, including (a) sample pH value, (b) sample flow rate, (c) TU concentration (m/v) and (d) eluent flow rate.

absorbances of Au, Pd and Pt were obtained with 0.1 mol L^{-1} HCl. Considering that the graphite tube exhibits low tolerance to the strong acidity, an eluent solution containing 2.0% TU and 0.1 mol L^{-1} HCl was the most suitable eluent for the desorption of analytes and it was used as the eluent in the following experiments.

3.2.6. Effect of eluent flow rate

To investigate the influence of eluent flow rate on the absorbance, flow rates varying in the range of 0.5–4.0 mL min^{-1} were studied. Fig. 6d indicates that the absorbance decreased evidently when the eluent flow rate increased, because high flow rate generally led to a loss in contact time between the metal ions and the eluent. However, the eluent flow rate lower than 0.5 mL min^{-1} was not adopted because the precision of determination decreased slightly. Therefore, 1.0 mL min^{-1} was used for further experiments.

3.3. Analytical figures of merit

Under the optimized conditions, a series of experiments have been carried out to evaluate the proposed method. The calibration curve was obtained after the standard solution was injected in the FI-column-GFAAS system. The correlation coefficients (R^2) values were 0.9991, 0.9999, and 0.9994 for Au, Pd, and Pt, respectively. The enrichment factor (EF), calculated by the ratios between the slopes of the calibration curves with and without the on-line preconcentration step, was determined as 24.3 for Au, 13.9 for Pd, and 17.8 for Pt. According to the IUPAC recommendations, LOD was calculated as three times the standard deviation of the blank signals. Under optimum conditions, the LOD values for Au, Pd, and Pt were 0.16, 0.28, and 1.01 ng mL^{-1}. The relative standard deviations (RSD) of our method, obtained for seven determinations of Au, Pd, and Pt were 1.1%, 3.9%, and 4.4%, respectively. All the characteristic data for the analytical performance are summarized in Table 2.

Table 2
Analytical characteristics of the method.

Element	Linear range (ng mL^{-1})	R^2	LOD (ng mL^{-1})	LOQ (ng mL^{-1})	%RSD ($n=7$)	EF
Au	0.5 – 3	0.9991	0.16	0.53	1.1	24.3
Pd	0.5 – 8	0.9999	0.28	0.93	3.9	13.9
Pt	1.5 – 20	0.9994	1.01	3.36	4.4	17.8

As a comparison, some reported on-line preconcentration procedures for the determination of precious metals are summarized in Table 3. The present strategy cannot provide the best LOD level. However, it is comparable when considering not only the analytical characteristics but also its advantage of lower capital of operational cost compared with some other pretreatment techniques. Furthermore, the present method is environment friendly because of its solvent-free characteristics.

3.4. Analysis of real samples

In order to validate the accuracy and applicability of proposed method, four certified reference materials (GAu-11b, GBW07289, GBW07291, and GBW07292), were analyzed for their precious metal concentrations. As shown in Table 4, no significant differences were observed between the certified and found values, illustrating the determined values of the present method agree well with the certified values.

Under the recommended experimental conditions, mine samples were analyzed to verify the applicability of the developed method. All the samples were spiked with Au, Pd, and Pt standard solutions. The results are shown in Table 4. The recovery values demonstrated that a sufficient recovery could be achieved in the range of 89.6–111.2%, demonstrating that the developed method could be used for the determination of Au, Pd, and Pt in mine samples.

4. Conclusion

The coupling of flow injection on-line separation and preconcentration of trace elements with graphite furnace atomic absorption spectrometry (FI-column-GFAAS) was proved to be a feasible technique for determination of precious metals in mine samples. A novel superparamagnetic adsorbent, crown ether-functionalized magnetic silica nanoparticle, was successfully synthesized and characterized. The combination of FI-column and GFAAS for Au, Pd, and Pt determination allowed the detection limits of 0.16, 0.28, and 1.01 ng mL^{-1}, which enabled low levels of these elements to be determined. In addition, excellent analytical characteristics such as high enrichment factor, high sensitivity, and accuracy for the determination, proved a promising application of the method for trace Au, Pd, and Pt analysis.

Table 3
Summary of some established on-line preconcentration methods for precious metals determinations.

Ion	Adsorbent	Instrument	Linear range (ng mL^{-1})	LOD (ng mL^{-1})	%RSD	Application	Ref.
Au, Pd	Duolite GT-73	ICP-OES	–	0.085, 0.28	0.5–3	Electrolytic bath samples	[5]
Pd, Pt	Metalfix-chelamine resin	ICP-OES	0–100, 0–2000	0.0025, 0.022	1–3	Pellet automobile catalysts	[6]
Pd, Pt	Alumina	ICP-OES	0–150	0.7, 2.1	2–7	Roadside soils	[7]
Pd	PANI	ICP-MS	0–100	0.0004	<3	Water samples	[8]
Pd, Pt	PSTH-CPG	ICP-MS	0–0.6	0.0555, 0.0785	3	Environmental samples	[9]
Au, Pd, Pt	Mercapto-functionalized magnetite microspheres	ICP-MS	1700–2500	0.0017, 0.0018, 0.0019	1.2–2.1	–	[10]
Pd	DKTS-APSG resin	FAAS	–	5.0	<2	Tap water, catalytic converter	[23]
Pd	Poly(DPMAAm-*co*-DVB-*co*-AMPS) chelating resin	FAAS	1000–12,000	1.7	2.8	Water, cream, anode slime, converter samples	[24]
Pd	Alumina/PEI	FAAS	100–8000	0.042	2.3	Standard alloy, anodic slime	[25]
Pd	C18 /DEBT	GFAAS	0–2	0.023	3.9	Aerosol samples	[26]
Pd	PSTH/Dowex 1 × 8–200	GFAAS	–	2	3.57	Water, vegetation, soil, foods	[3]
Au, Pd, Pt	CEMNs	GFAAS	0.5–3, 0.5–8, 1.5–20	0.16, 0.28, 1.01	1.1–4.4	Mine samples	This work

Table 4
Determination results of Au, Pd, and Pt in certified reference materials and mine samples (mean ± S.D., $n=3$).[a]

	Au	Pd	Pt
GAu-11b			
Certified (ng g^{-1})	10.5 ± 0.5	–	–
Measured (ng g^{-1})	11.1 ± 0.3	–	–
GBW07289			
Certified (ng g^{-1})	10 ± 2	2.3 ± 0.2	1.6 ± 0.3
Measured (ng g^{-1})	11 ± 0.4	2.1 ± 0.1	1.3 ± 0.5
GBW07291			
Certified (ng g^{-1})	4.3 ± 0.3	60 ± 9	58 ± 5
Measured (ng g^{-1})	4.7 ± 0.3	61 ± 3	57 ± 4
GBW07292			
Certified (ng g^{-1})	–	11.3 ± 1.5	20 ± 4
Measured (ng g^{-1})	–	10.3 ± 0.7	18 ± 1
Sample 1			
Measured (ng g^{-1})	7.05	4.18	14.80
Found (ng g^{-1})	12.48	9.44	20.36
Recovery (%)	108.5	105.1	111.2
Sample 2			
Measured (ng g^{-1})	6.23	< LOD	< LOD
Found (ng g^{-1})	10.99	4.48	5.22
Recovery (%)	95.2	89.6	104.4
Sample 3			
Measured (ng g^{-1})	5.43	1.77	< LOD
Found (ng g^{-1})	10.35	6.85	5.38
Recovery (%)	98.3	101.5	107.5

[a] The concentrations of Au, Pb, and Pt spiked to mine samples are all 5 ng g^{-1}.

Acknowledgment

The project was supported by the State Key Laboratory of Inorganic Synthesis and Preparative Chemistry, College of Chemistry, Jilin University (2012–16).

References

[1] B. Salih, O. Celikbicak, S. Doker, M. Dogan, Anal. Chim. Acta 587 (2007) 272–280.
[2] G.Z. Tsogas, D.L. Giokas, A.G. Vlessidis, N.P. Evmiridis, Talanta 76 (2008) 635–641.
[3] C.B. Ojeda, F. Sanchez Rojas, J.M. Cano Pavon, Microchim. Acta 158 (2007) 103–110.
[4] M. Shamsipur, M. Ramezania, Talanta 75 (2008) 294–300.
[5] P. Pohl, B. Prusisz, Microchim. Acta 150 (2005) 159–165.
[6] M. Muzikar, C. Fontas, M. Hidalgo, J. Havel, V. Salvado, Talanta 70 (2006) 1081–1086.
[7] E. Herincs, M. Puschenreiter, W. Wenzel, A. Limbeck, J. Anal. At. Spectrom. 28 (2013) 354–363.
[8] M.V. Balarama Krishna, M. Ranjit, K. Chandrasekaran, G. Venkateswarlu, D. Karunasagar, Talanta 79 (2009) 1454–1463.
[9] M.L. Alonso Castillo, A. Garcia de Torres, E. Vereda Alonso, M.T. Siles Cordero, J. M. Cano Pavon, Talanta 99 (2012) 853–858.
[10] Y. Li, Y.F. Huang, Y. Jiang, B.L. Tian, F. Han, X.P. Yan, Anal. Chim. Acta 692 (2011) 42–49.
[11] G. Weber, H. Messerschmidt, Anal. Chim. Acta 545 (2005) 166–172.
[12] M. Constantin, J. Radioanal. Nucl. Chem. 267 (2006) 407–414.
[13] A. Ramesh, H. Hasegawa, W. Sugimoto, T. Maki, K. Ueda, Bioresour. Technol. 99 (2008) 3801–3809.
[14] A. Arcadi, Chem. Rev. 108 (2008) 3266–3325.
[15] N. Das, Hydrometallurgy 103 (2010) 180–189.
[16] L. Liu, C. Li, C.L. Bao, Q. Jia, P.F. Xiao, X.T. Liu, Q.P. Zhang, Talanta 93 (2012) 350–357.
[17] M. Soylak, M. Tuzen, J. Hazard. Mater. 152 (2008) 656–661.
[18] M. Shamsipur, M. Ramezani, M. Sadeghi, Microchim. Acta 166 (2009) 235–242.
[19] T.R. Reddy, N.N. Meeravali, A.V.R. Reddy, Sep. Purif. Technol. 103 (2013) 71–77.
[20] S.X. Chen, R. Xu, H.X. Huang, F.Y. Yi, X. Zhou, H.M. Zeng, J. Mater. Sci. 42 (2007) 9572–9581.
[21] D.D. Li, X.J. Chang, Z. Hu, Q.H. Wang, Z.F. Tu, R.J. Li, Microchim. Acta 174 (2011) 131–136.
[22] X.Q. Chen, K.F. Lam, S.F. Mak, K.L. Yeung, J. Hazard. Mater. 186 (2011) 902–910.
[23] R.K. Sharma, A. Pandey, S. Gulati, A. Adholeya, J. Hazard. Mater. 209 (2012) 285–292.
[24] T. Cetin, S. Tokalioglu, A. Ulgen, S. Sahan, I. Ozenturk, C. Soykan, Talanta 105 (2013) 340–346.
[25] F. Sabermahani, M.A. Taher, J. Anal. At. Spectrom. 25 (2010) 1102–1106.
[26] A. Limbeck, J. Rendl, H. Puxbaum, J. Anal. At. Spectrom. 18 (2003) 161–165.
[27] Y.F. Sha, C.H. Deng, B.Z. Liu, J. Chromatogr. A 1198 (2008) 27–33.
[28] G. Morales-Cid, A. Fekete, B.M. Simonet, R. Lehmann, S. Cardenas, X.M. Zhang, M. Valcarcel, P. Schmitt-Kopplin, Anal. Chem. 82 (2010) 2743–2752.
[29] X.L. Zhang, H.Y. Niu, Y.Y. Pan, Y.L. Shi, Y.Q. Cai, Anal. Chem. 82 (2010) 2363–2371.
[30] Y.H. Deng, D.W. Qi, C.H. Deng, X.M. Zhang, D.Y. Zhao, J. Am. Chem. Soc. 130 (2008) 28–29.
[31] M.H. Mashhadizadeh, M. Amoli-Diva, J. Anal. At. Spectrom. 28 (2013) 251–258.
[32] J.J. Ye, W. Feng, M.M. Tian, J.L. Zhang, W.H. Zhou, Q. Jia, Anal. Methods 5 (2013) 1046–1051.
[33] M.C. Bruzzoniti, R.M. De Carlo, M. Fungi, J. Sep. Sci. 31 (2008) 3182–3189.
[34] B. Mokhtari, K. Pourabdollah, J. Incl. Phenom. Macrocycl. Chem. 73 (2012) 269–277.
[35] G. Ekmekci, D. Uzun, G. Somer, S. Kalayci, J. Membr. Sci. 288 (2007) 36–40.
[36] M. Chamsaz, M.H. Arbab-Zavar, A. Darroudi, T. Salehi, J. Hazard. Mater. 167 (2009) 597–601.
[37] P.D. Beer, P.K. Hopkins, J.D. McKinney, Chem. Commun. (1999) 1253–1254.
[38] Y. Li, B. Yan, C.H. Deng, W.J. Yu, X.Q. Xu, P.Y. Yang, X.M. Zhang, Proteomics 7 (2007) 2330–2339.
[39] L. Ferreira, M.A. Ramos, M.H. Gil, J.S. Dordick, Biotechnol. Prog. 18 (2002) 986–993.
[40] W.S. Price, F. Hallberg, P. Stilbs, Magn. Reson. Chem. 45 (2007) 152–156.
[41] D. Sahin, Z. Hayvali, J. Incl. Phenom. Macrocycl. Chem. 72 (2012) 289–297.
[42] T. Ogata, Y. Nakano, Water Res. 39 (2005) 4281–4286.
[43] S. Morisada, Y.H. Kim, T. Ogata, Y. Marutani, Y. Nakano, Ind. Eng. Chem. Res. 50 (2011) 1875–1880.